Journal of Nuclear Materials 406 (2010) 212–217

Contents lists available at ScienceDirect

Journal of Nuclear Materials

journal homepage: www.elsevier.com/locate/jnucmat

Threshold stress intensity factor for delayed hydride cracking of a recrystallized N18 alloy plate along the rolling direction

Chao Sun [a,*], Jun Tan [a], Shihao Ying [a], Qian Peng [a], Cong Li [b]

[a] National Key Laboratory for Nuclear Fuel and Materials, Nuclear Power Institute of China, P.O. Box 436, Chengdu 610041, China
[b] Department of R&D, State Nuclear Power Technology Corporation Limited, Beijing

ARTICLE INFO

Article history:
Received 21 September 2009
Accepted 25 August 2010

ABSTRACT

The objective of this study is to obtain the threshold stress intensity factor, K_{IH}, for an initiation of delayed hydride cracking in a recrystallized N18 (Zr–Sn–Nb–Fe–Cr) alloy plate which was manufactured in China, gaseously charged with 60 ppm of hydrogen by weight. By using both the load increasing method and load drop method, the K_{IH}'s along the rolling direction were investigated over a temperature range of 150–255 °C. The results showed that K_{IH} along the rolling direction was found to be higher in the load increasing method than that in the load drop method. In the load increasing method, K_{IH}'s of the N18 alloy plate appeared to be in the range of 31—32.5 MPa$\sqrt{m}$, and K_{IH} in the load drop method appeared to be in the range of 27.5—28.6 MPa$\sqrt{m}$. This means that the N18 alloy plate has high tolerance for DHC initiation along the rolling direction. The texture of a N18 alloy plate was investigated using an X-ray diffraction and the K_{IH} was discussed based on texture and analytically as a function of the tilting angle of hydride habit planes to the cracking plane.

1. Introduction

Zirconium alloys has been successfully used as cladding and structural materials in light and heavy water nuclear reactors for many years because of their low capture cross-section for thermal neutrons and good mechanical and corrosion properties. During their service a part of hydrogen produced through the corrosion reaction of Zr with hot coolant is absorbed by materials. Hydrogen in excess of solid solubility precipitates out as hydride phase of platelet morphology and could make the host matrix brittle. Hydride induced embrittlement significantly influences the in-service performance of the Zr-alloys components. Delayed hydride cracking (DHC) is a localized form of hydride embrittlement, which in the presence of a tensile stress-field manifests itself as a subcritical crack growth process. Consequently, hydrogen atoms in the solid solution will diffuse into the region that is ahead of the crack tip when it is subjected to a triaxial state of stress, which may lower the chemical potential of hydrogen in the region ahead of the crack tip. Once the hydrogen concentration in this region reaches (or exceeds) the terminal solid solubility for precipitation (TSSP), hydrides will start to form and grow. When the hydrides at the crack tip reach a critical size, the main crack will propagate through this hydrided region. The crack front finally is arrested at the end of the hydrided region by the ductile zirconium matrix, and the whole process repeats itself [1–4]. DHC was the cause of leakage in some Zr–2.5Nb pressure tubes of CANDU plants at Pickering and Bruce [5] and Russian RMBK reactors at Kursk and Chernobyl [6] and may contribute to the large axial splits experienced in the Zircaloy fuel cladding in light water reactors [7,8].

The threshold stress intensity factor (K_{IH}) is an important parameter for an evaluation of the integrity of the Zr-alloy components of a reactor, because it can be used to determine whether stable DHC crack growths start [3,9]. Although the threshold stress intensity factor has been studied for a long time, most of them were performed on Zr–2.5Nb and Zircaloy-2 [1–6,9–13] and few literatures were found on the subject of K_{IH} in Zircaloy-4 [4,14]. Almost no information was found on Zr–Sn–Nb alloy. Currently, several new Zr-based alloys have been developed from the point of view of enhancement of corrosion resistance and hydrogen pickup properties as a substitute for Zircaloy [15–17]. In China, N18 (Zr–Sn–Nb–Fe–Cr) alloy have been developed on the base of Zr–Sn and Zr–Nb systems to meet the requirements of higher fuel burn-up [18–21]. Up to now, we have not any DHC data for a N18 alloy plate, moreover, anisotropic DHC properties (including K_{IH}) of Zr–Nb alloys and Zircaloy-2 were found [22,23,33]. Therefore, systematic DHC properties data along all directions for a N18 alloy plate are needed. And based on the systematic DHC properties data we will establish a database related to DHC of the N18 alloy plate.

The purpose of the present study was to investigate the threshold stress intensity factor for delayed hydride cracking of a N18

* Corresponding author. Tel.: +86 28 8590 3294.
E-mail address: sunchaonpic@yahoo.com.cn (C. Sun).

0022-3115/$ - see front matter © 2010 Elsevier B.V. All rights reserved.
doi:10.1016/j.jnucmat.2010.08.025

alloy plate along the rolling direction for the first time. The present study will contribute to the establishment of a database related to DHC of the N18 alloy plate and it is a part of the systematic DHC behaviors for the N18 alloy plate. In the present investigation, by using both the load increasing method (LIM) and load drop method (LDM), we determined K_{IH} along the rolling direction over a temperature range of 150–255 °C. The fracture surfaces were examined by using the scanning electron microscope (SEM).

2. Experimental procedures

2.1. Specimen preparation

The vacuum consumable arc remelting method was employed for producing 500 kg ingot of Zr–Sn–Nb–Fe–Cr zirconium alloy with the chemical compositions (in wt.%): Sn: 1.05; Nb: 0.27; Fe: 0.35; Cr: 0.1; O: 0.09; Zr: balance. β-Quenching treatment in water was conducted to homogenize the composition within the ingot after being hot forged. Then the ingot was made into plates of about 4.6 mm thickness through various rolling and intermediate annealing (600 °C) processes. The final annealing was conducted at 580 °C for 2 h in vacuum [18,24,25]. The equiaxed grains were measured to be about 10 μm in diameter. The room temperature yield strength and ultimate tensile strength of N18 alloy plate along the rolling direction was 419 and 535 MPa respectively [25]. The texture of N18 alloy plate was confirmed by (0 0 0 2) pole figure measurement using an X-ray diffraction (XRD). The N18 alloy plate presents a bimodal distribution of the intensity maxima, and it exhibits a strong texture with a maximum (0 0 0 2) pole density at ~25° toward the transverse direction from the plate normal, as shown in Fig. 1 where the rolling and transverse directions are denoted as RD and TD, respectively. The basal pole components of the N18 alloy plate are shown in Table 1. The basal pole components in the rolling direction and transverse direction are lower than that along plate normal obviously.

Seventeen millimeter compact tension (CT) specimens shown in Fig. 2 which were manufactured in accordance with ASTM standard test method (E-399) were used to determine K_{IH} along the rolling direction. The CT specimens were charged with hydrogen using a gaseously hydrided method and a diffusion annealing treatment was performed to obtain about 60 ppm of hydrogen throughout the specimens. More details of the hydrogen charging procedure are reported elsewhere [25]. The real hydrogen content of the specimen was obtained by averaging a set of two data measured with a LECO RH 600 hydrogen analyzer. The CT specimens were then fatigue pre-cracked to obtain a sharp crack tip and uniform crack front at room temperature, an initial crack length of about 1.7 mm. The stress intensity factor, K_I, was calculated using the following Eqs. (1) and (2) from ASTM E-399:

$$K_I = P_Q/(B \times W^{1/2}) \times f(a/W) \quad (1)$$

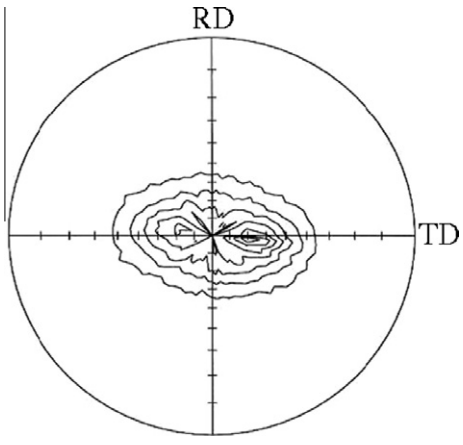

Fig. 1. (0 0 0 2) Pole figures for a N18 alloy plate.

Table 1
The basal pole components in N18 alloy plate.

Specimens	Basal pole components		
	Rolling direction, F_R	Transverse, F_T	Plate normal, F_N
N18 alloy plate	0.09	0.16	0.75

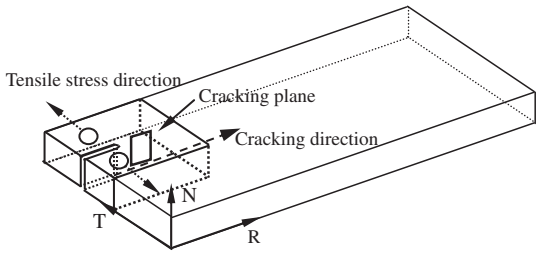

Fig. 2. Schematic illustration of a compact tension specimen and the orientation of the cracking plane.

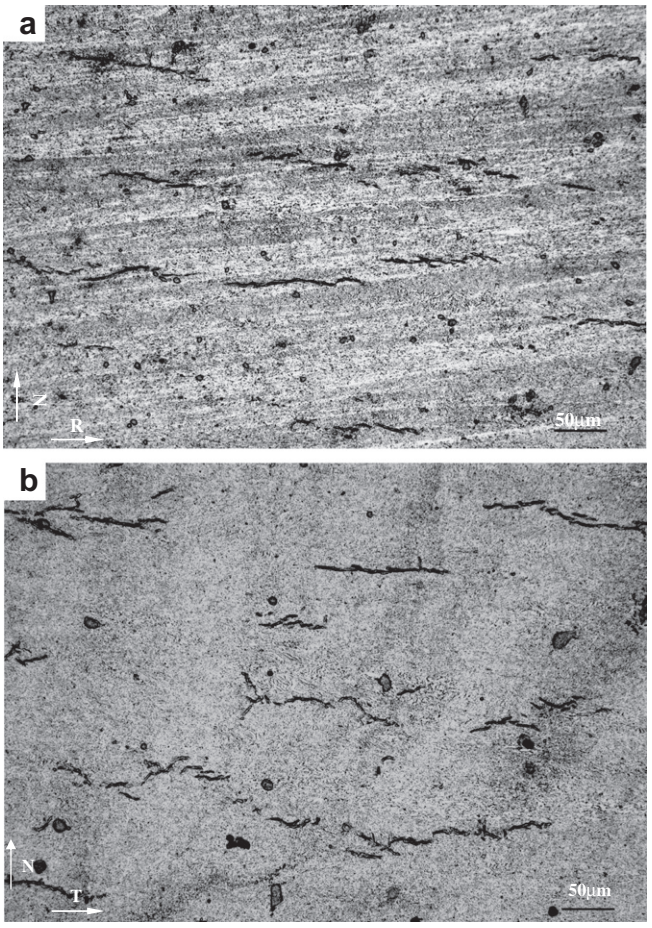

Fig. 3. Hydride morphology of a N18 alloy plate with 60 ppm (a) RD–ND plate and (b) TD–ND plate.

$$f(a/W) = (2 + a/W)[0.886 + 4.64(a/W) - 13.32(a/W)^2 + 14.72(a/W)^3 - 5.6(a/W)^4]/(1 - a/W)^{3/2} \quad (2)$$

where P_Q = applied load (N), B = specimen thickness (m), W = specimen width (m), a = crack length (m).

The hydride morphology was observed with an optical microscopy. The typical metallography of hydride structure on the rolling-normal plane and transverse-normal plane were depicted in Fig. 3a and b, revealed that hydrides (dark lines) were appeared as a line segment and uniformly distributed.

2.2. Delayed hydride cracking tests

A CSS-250 creep testing machine was used to carry out DHC tests. The equipment consisted of single arm lever type loading system fitted with a resistance heated two zone furnace to provide temperature control within 1 °C of the set temperature. The lever arm ratio of the loading system was 1:10. The temperature of the specimen was monitored using K-type thermocouple spot welded to the surface of the specimen within 2 mm of the fatigue pre-crack tip. The DHC crack growth was monitored using direct current potential drop (DCPD) technique using a DC constant-current power source [12]. The temperature output from the thermocouple and DCPD signal were continuously recorded every minute using computer data acquisition system [25].

A schematic diagram of thermal cycle which the CT specimens experienced in the DHC tests was shown in Fig. 4. The CT specimens were heated to a peak temperature at a heating rate between 2–3 °C/min, held at peak temperature for 90 min and cooled down to the test temperature followed by applying a load 30 min after attaining the test temperature. The peak temperature was set at 330 °C, which was about 50 °C higher than the terminal solid solubility for dissolution (TSSD) temperature to dissolve all the charged hydrogen in the zirconium matrix. In the LIM, the initial applied load, which corresponded to a stress intensity factor (SIF) of 20 MPa$\sqrt{m}$, was increased step-wise to ensure increase in SIF of 1 MPa$\sqrt{m}$ when the crack did not grow within 24 h. In contrast, in the LDM, the first step of tests in the investigation was performed at the highest applied load, which corresponded to an SIF of 35 MPa$\sqrt{m}$. DHC crack growth under constant load was monitored by DCPD technique and after obtaining a crack growth of some finite distance (of the order of 100 μm), the load was reduced to ensure decrease in SIF of 1 MPa$\sqrt{m}$ (after each successive load drop, the updated value of crack length and geometrical factor was used to compute K_I) and the same sequence was repeated till a K_I was reached which produced insignificant change in DCPD signal as a function of time for 24 h. The final K_{IH} was calculated using the final crack length after breaking the specimen. Duplicate tests were carried out at each test temperature to ensure the reliability of the K_{IH} data.

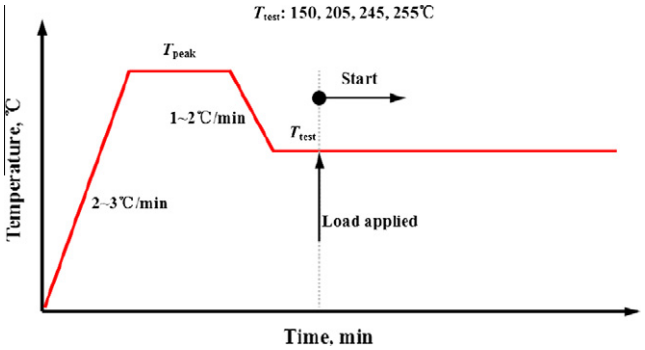

Fig. 4. Schematic diagram of a thermal cycle during the DHC tests.

3. Results and discussion

3.1. K_{IH} along the rolling direction with both LIM and LDM

Fig. 5a shows a typical plot of DCPD output and specimen temperature as a function of time during the LIM testing carried out at 205 °C corresponding to one constant load. As can be seen in this figure, for all the tests the specimen temperatures remained constant throughout the DHC testing. The slope of DCPD versus time curve increased with time. These indicated that the DHC crack growth rate was increased slightly with an increasing DHC crack length. A typical plot of DCPD output and load as a function of time during the LIM testing carried out 205 °C was depicted in Fig. 5b, revealed that significant incubation period of DHC were observed. Fig. 6a shows changes of DCPD output and specimen temperature with time during the LDM testing carried out 245 °C corresponding to variation of load. A plot of load drop step and the corresponding change in DCPD output with time carried out 245 °C are shown in Fig. 6b. In the LDM, the slope of DCPD versus time curve decreased with a decreasing load, which indicated that the DHC crack growth rate was decreased with a decreasing the applied K_I.

The threshold stress intensity factor K_{IH} were determined for the N18 alloy plate specimens by plotting the measured crack velocity as a function of stress intensity factor as shown in Fig. 7. As expected, the stress intensity factor $(K_I) > 29$ MPa$\sqrt{m}$, DHC velocity is practically independent of the former and below this value DHC velocity decreases with decrease in K_I. The threshold stress intensity factors, K_{IH}'s of the N18 alloy plate along the rolling

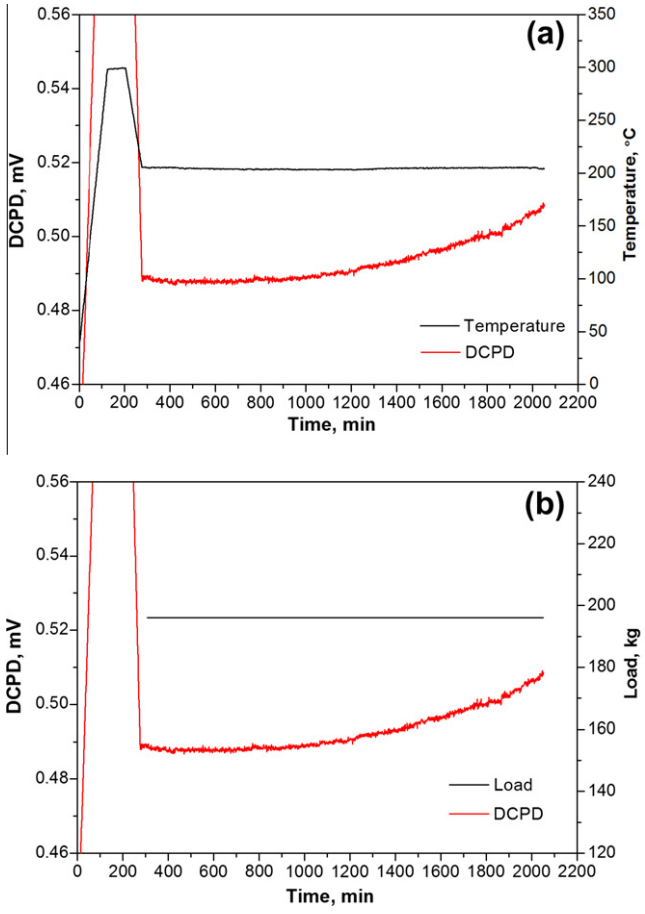

Fig. 5. (a) A plot of DCPD output and specimen temperature against time obtained during the LIM test carried out at 205 °C and (b) a typical plot of DCPD output and load as a function of time during the LIM test carried out at 205 °C.

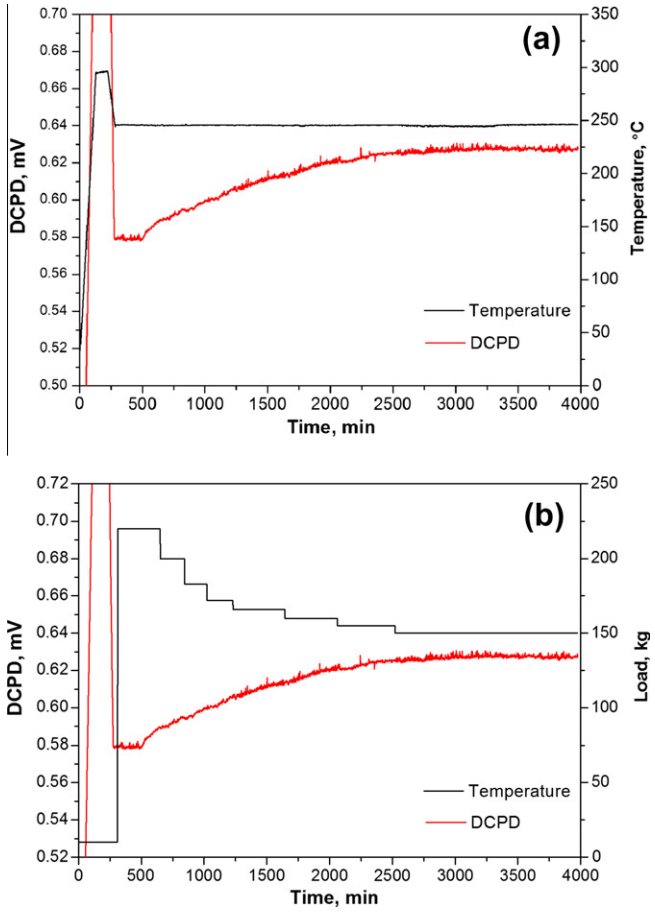

Fig. 6. (a) A typical plot of DCPD output and specimen temperature as a function of time during the LDM test carried out at 245 °C and (b) a typical load drop step and corresponding change in DCPD output with time during the LDM test carried out at 245 °C.

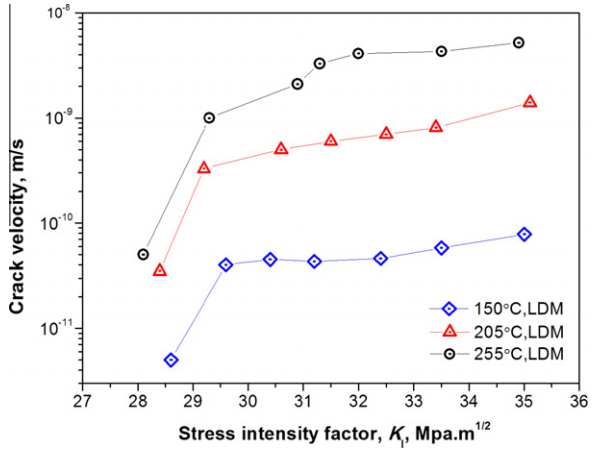

Fig. 7. Crack velocity as a function of stress intensity factor for N18 alloy plate at various temperatures.

direction obtained using both LIM and LDM were plotted in Fig. 8. K_{IH} of the N18 alloy plate along the rolling direction was found to be higher in the LIM than that in the LDM over a temperature range of 150–255 °C. In the LIM, K_{IH}'s of the N18 alloy plate appeared to be in the range of 31—32.5 MPa$\sqrt{m}$, and K_{IH} in the LDM appeared to be in the range of 27.5—28.6 MPa$\sqrt{m}$. A higher K_{IH} in the LIM,

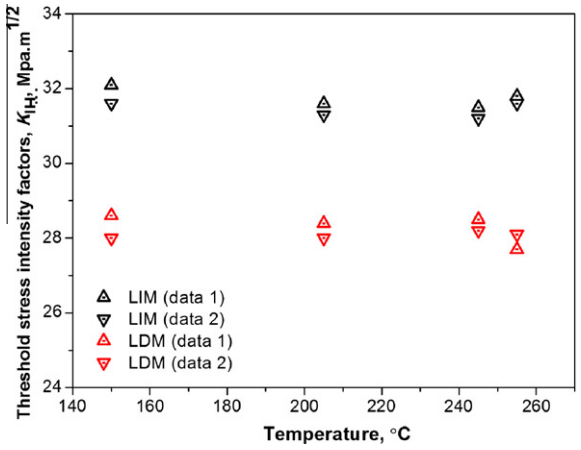

Fig. 8. Threshold stress intensity factors, K_{IH}'s of N18 alloy plate containing 60 ppm H with temperature and with the loading modes.

shown in Fig. 8, may be partly due to a different crack tip size contingent on the loading modes. It should be noted that the initial crack, growing in the LIM, is a pre-fatigue crack that was formed at a larger K_I of 32.5 MPa$\sqrt{m}$ but the grown crack in the LDM is a DHC crack that must have been created at a lower K_I of around 28.5 MPa$\sqrt{m}$. Considering that the DHC crack grows at a lower K_I than the fatigue crack, the tip of the DHC crack would be sharper than that of the fatigue crack, leading to a lower level of stress ahead of the tip of the fatigue crack [23,26]. The threshold behavior for N18 alloy plate revealed that K_{IH}'s of the N18 alloy plate remained constant in a temperature range of 150–255 °C in the LDM while they slightly decreased with an increasing temperature in the LIM. This is due to the different temperature dependencies of K_{IH} contingent upon the loading modes: A slightly decrease of K_{IH} with increasing temperature in the LIM is likely due to the increased number of twins at a temperature range of 150–255 °C. The higher the number of twins, the easier cracking of the hydrides and the lower K_{IH} in the LIM becomes [9]. This strong dependency of K_{IH} on the number of twins seems to arise from some difficulties in cracking of the grown hydrides by twins part of which are suppressed by prior creep deformation and thereby causing a blunt crack tip only in the load-increasing mode. By contrast, in the LDM, the hydrides which precipitate in the plastic zone grow long enough to exceed critical hydride length even without creep, and the crack front is very sharp, causing the hydrides to fracture more easily by the twin–hydride interactions. Thus, the number of twins is not so critical in determining K_{IH} as long as there are a few twins for inducing cracking of the hydrides, leading to a constant K_{IH} independent of the number of the twins over a temperature range of 150–255 °C.

It is noted that the K_{IH} values along the rolling direction of a recrystallized N18 alloy plate with both LIM and LDM in this study are higher than the previous data. This means that the N18 alloy plate along the rolling direction is not susceptible to cracking by DHC. Many studies [27–33] focused on the K_{IH} in various Zr-alloys, and confirmed that K_{IH} is practically independent of material strength and the minimum alloying elements in zirconium. However, because of the anisotropy of hexagonal α-zirconium, a texture is formed upon plastic deformation during the fabrication process, which will effect hydride precipitation. Since the DHC crack grows by fracturing of hydrides, an initiation of the DHC crack would depend strongly on the orientation of the hydride habit plane where the hydrides can precipitate preferentially. In other words, if the hydride habit plane is parallel to the cracking plane, the DHC crack initiation will be easy. On the contrary, where the hydride habit plane is tilting from the cracking plane, the crack

initiation will be difficult, leading to an increase in threshold stress intensity factor, K_{IH}, or to an increase in DHC resistance. Cheadle et al. [28] pointed out that hydride reorientation will become easier if their basal plane normals are parallel to the tensile stress. In this situation, the reoriented hydride platelets will be parallel to the basal plane of α-zirconium. Since the effective hydride platelets during the DHC process are those reoriented ones, the relative orientation between the basal plane of α-zirconium and the cracking plane will be an important factor in DHC initiation and propagation. Therefore, Coleman et al. [29] proposed that if the crystallographic texture can be arranged so that the basal plane normals of α-grains are nearly perpendicular to the major tensile stress, DHC can be diminished. Thus, DHC behavior is closely related to the texture of Zr-alloys. Since $\{10\bar{1}7\}$ planes are the most favorable habit planes for the precipitation of hydrides in zirconium alloys under tensile stress [3,28,34–36], the initiation of DHC may depend strongly on the available number of the habit planes that is determined by texture. So we speculated that the higher K_{IH} values along the rolling direction of a N18 alloy plate may be owing to the texture of the N18 alloy plate. We will discuss in detail in Section 3.2.

3.2. Effect of texture

The K_{IH} is a critical K_I value over which the crack grows physically through the DHC mechanism. The DHC mechanism involves the kinetics of the formation of the hydride, namely, the diffusion of hydrogen to the crack tip region and the precipitation of the hydride and its fracture under the given loading condition. When the applied load is constant, then the applied K_I at the crack tip will be constant. Only the precipitation of the hydride at the crack tip will be changed with time. The load enduring capability will be decreased with an increased fraction of the hydride at the crack tip. If the applied load or stress at the crack tip exceeds the load enduring capability with the aid of the hydride at the crack tip, a certain length of the mixture of the hydride and matrix will be fractured simultaneously, and this process will be repeated. This is the very mechanism of a DHC. Therefore, there might be inherent K_{IH} values of a given texture, according to the distribution of the basal planes or the habit plane of the hydride, $\{10\bar{1}7\}$. So some studies focused on the effect of texture variation on the DHC behaviors [29,30,34–37] and had confirmed that the K_{IH} decreases linearly with a basal pole component (F) oriented along crack plane normal in various Zr-alloy plates and tubes, as shown in Fig. 9. This shows that there is a significant texture dependence regardless of the materials. This is due to the fact that the major phase is α-Zr in zirconium alloys.

The decreasing K_{IH} trend with F was explained by the rule of a mixture [3,36]. The volume fraction of the ductile matrix can be assumed as $(1-F)$ and that of the brittle hydride can be assumed as F, because the physical meaning of F is the resolved fraction of the basal plane in the cracking plane. The texture dependence of K_{IH} can be expressed by the following Eq. (3) [3,36].

$$K_{IH} = (1-F) \times K^*_{IH} + F \times K_{IC}, \tag{3}$$

where K^*_{IH} is the fracture toughness of a complete ductile matrix containing hydrogen at $F = 0$, and K_{IC} is the fracture toughness of hydride which is reported as K_{IC} = 1–3 MPa $\sqrt{m}$ [3,36]. The increase in F in the cracking plane reduces the area of the ductile matrix. This means that the plane having a higher F has a lower resistance to a DHC. Therefore, if F for the cracking plane is higher, then the K_{IH} is lower; the K_{IH} decreases with F, and vise versa.

The K_{IH} of N18 alloy plate along the rolling direction is plotted against the basal pole component in Fig. 9. This shows that the trend is consistent with the literature. The relationship between tensile stress direction, the cracking direction and the cracking plane in the CT specimens is shown in Fig. 2. In the present study, (0 0 0 2) poles in the N18 alloy plate are concentrated in the plate normal, as discussed above. It is known that DHC in Zr-alloys occurs due to the repetition of precipitation of brittle hydrides and their fracture when the hydrogen content is over TSS (terminal solid solubility) at the temperature of the system, and that hydrides precipitate on the habit planes $\{10\bar{1}7\}$ under tensile stress, and the crack grows by hydrides precipitated on the habit planes, which are tilted by 15° from the basal plane (0 0 0 2) [3,34,35,37,38]. However, in the case of the CT specimens, the cracking plane is along RD–ND plate. The interplanar angle between the cracking plane of the CT specimen and the habit plane of the hydride is ~75°. Therefore, there is lower number of grains having habit plane for the hydride near or parallel to the cracking plane. This is why the CT specimens along the rolling direction are difficult to crack by a DHC. It is natural, that K_{IH} for DHC initiation in the rolling direction is higher than the previous data. This means that the N18 plate in rolling direction has a higher resistance to a DHC.

3.3. SEM fractography

The low magnification fractograph are compared in Fig. 10. They illustrate the typical DHC fracture patterns obtained in the LIM tests carried out at 205 °C. The characteristics of the DHC surfaces obtained in the LDM tests carried out at 245 °C and 255 °C respectively show larger depth variations and a portion of ductile fracture in Figs. 11 and 12. It is clear that the DHC surfaces are very

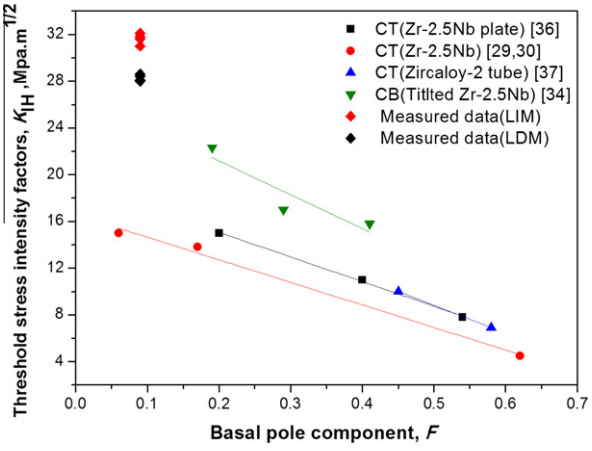

Fig. 9. The basal pole component (F) dependency of K_{IH} in various Zr-alloys.

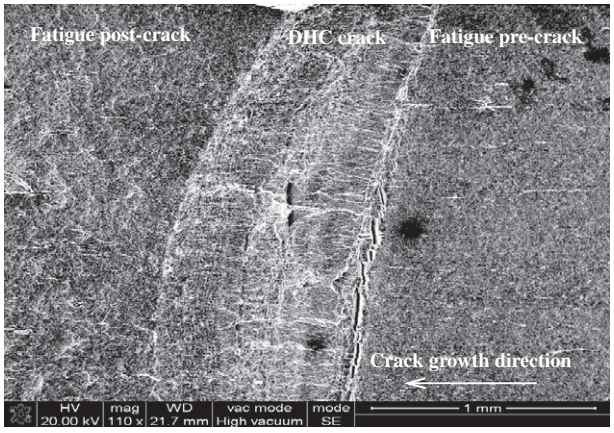

Fig. 10. Fractograph showing the fatigue pre-crack (FPC), DHC crack (D) and fatigue post-crack subjected to the LIM test carried out at 205 °C.

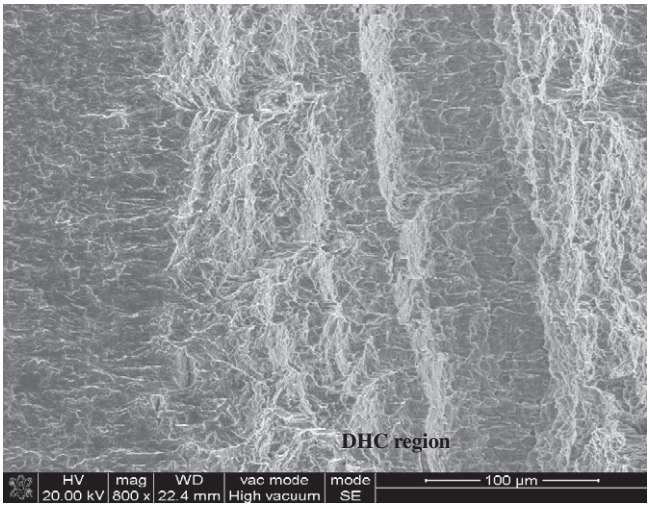

Fig. 11. A typical photograph of DHC fracture surface region subjected to the LDM testing carried out at 245 °C.

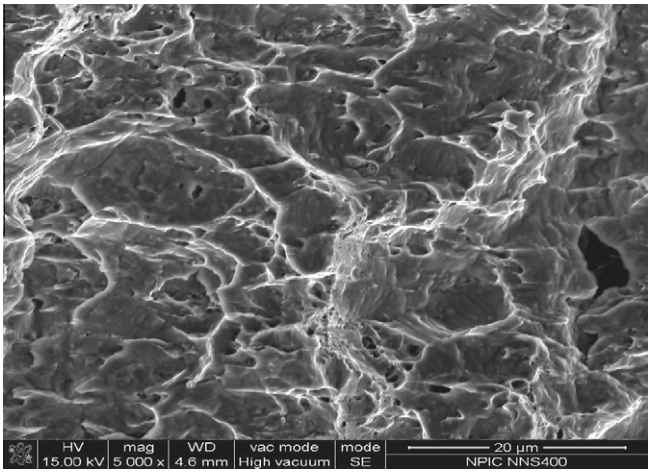

Fig. 12. A typical photograph of DHC fracture surface region subjected to the LDM testing carried out at 255 °C.

bumpy and show some chunky-wedges. This suggests that DHC cracking may encounter the lesser basal planes in the cracking plane and propagates through the various grain orientations. Then cracking is difficult, therefore, the required energy to propagate the DHC crack will be increased, and thus, it is the reason that the fracture surfaces are less smooth.

4. Conclusions

The threshold stress intensity factor (K_{IH}) values for an initiation of delayed hydride cracking (DHC) in a N18 (Zr–Sn–Nb–Fe–Cr) alloy plate which was manufactured in China were investigated for the first time. By using both the load-increasing mode (LIM) and load drop method (LDM), the load increasing method gives non-conservative results in comparison with the load drop method over a temperature range of 150–255 °C. In the LIM, K_{IH}'s of the N18 alloy plate appeared to be in the range of 31—32.5 MPa$\sqrt{m}$, and K_{IH} in the LDM appeared to be in the range of 27.5—28.6 MPa$\sqrt{m}$. This means that the plate normal textured of N18 alloy plate has high tolerance for DHC initiation along the rolling direction. The fact that the N18 alloy plate has a higher K_{IH} can be explained in terms of the lower basal plane density in the cracking plane. The characteristics of the DHC surfaces are very bumpy and show larger depth variations and a portion of ductile fracture. It is attributed to the less basal planes in the cracking plane.

Acknowledgements

The authors are grateful to National Key Laboratory for Nuclear Fuel and Materials to apply N18 alloy plate and DHC testing equipments. Furthermore, the authors are indebted to Professor Shihao Ying for suggestion of test and useful discussions.

References

[1] S.-Q. Shi, M.P. Plus, J. Nucl. Mater. 208 (1994) 232.
[2] Y.S. Kim, Y.G. Matvienko, Y.M. Cheong, S.S. Kim, S.C. kwun, J. Nucl. Mater. 278 (2000) 251.
[3] Sung Soo Kim, J. Nucl. Mater. 349 (2006) 83.
[4] J.-H. Huang, C.-S. Ho, Mater. Chem. Phys. 47 (1997) 184.
[5] Maria Roth, Rameshwar Choubey, Christopher Coleman, Iain Ritchie, in: Transactions of the Seventeenth International Conference on Structural Mechanics in Reactor Technology (SMiRT 17), Prague, Czech Republic, 2003, p. 17.
[6] P.A. Platonov, in: Eighth Conference on Zirconium in the Nuclear Industry, Available as AECL Report RC-87, ASTM, Philadelphia, 1988.
[7] D. Schrire, in: Proc. International Topical Meeting on Light Water Reactor Fuel Performance, ANS, West Palm Beach, 1994, p. 398.
[8] K. Edsinger, in: Twelfth Conference on Zirconium in the Nuclear Industry, ASTM STP 1354, ASTM, Philadelphia, 2000, p. 316.
[9] Y.S. Kim, Sun Sam Park, Sook In Kwun, J. Alloys Compd. 462 (2008) 367.
[10] R. Dutton, K. Nuttall, M.P. Puls, L.A. Simpson, Metall. Trans. A 8A (1977) 1553.
[11] Young Suk Kim, Sang Jai Kim, Kyung Soo Im, J. Nucl. Mater. 335 (2004) 387.
[12] R.N. Singh, Niraj Kumarb, R. Kishore, S. Roychaudhury, T.K. Sinha, B.P. Kashyap, J. Nucl. Mater. 304 (2002) 189.
[13] F.H. Huang, W.J. Millsm, Metall. Trans. A 22A (1991) 2049.
[14] J.-H. Huang, S.-P. Huang, Scr. Metall. Mater. 27 (1992) 1247.
[15] R.J. Comstock, G. Schoenberger, G.P. Sable, in: Eleventh Conference on Zirconium in the Nuclear Industry, ASTM STP 1295, ASTM, Philadelphia, 1996, p. 710.
[16] J.P. Mardon, D. Charquet, J. Senevat, in: Twelfth Conference on Zirconium in the Nuclear Industry, ASTM STP 1354, ASTM, Philadelphia, 2000, p. 505.
[17] A.V. Nikulina, V.A. Markelov, M.M. Peregud, Y.K. Bibilashvili, V.A. Kotrekhow, A.F. Lositsky, N.V. Kuzmenko, Y.P. Shevnin, V.K. Shamardin, G.P. Kobylyansky, A.E. Novoselov, in: Eleventh Conference on Zirconium in the Nuclear Industry, ASTM STP 1295, ASTM, Philadelphia, 1996, p. 785.
[18] Wenjin Zhao, Bangxin Zhou, Zhi Miao, Qian Peng, in: Thirteenth International Conference on Nuclear Engineering Beijing, China, 2005.
[19] W.Q. Liu, Q. Li, B.X. Zhou, Q.S. Yan, M.Y. Yao, J. Nucl. Mater. 341 (2005) 97.
[20] Y.Z. Liu, X.T. Zu, S.Y. Qiu, C. Li, W.G. Ma, X.Q. Huang, Surf. Coat. Technol. 200 (2006) 5631.
[21] W.J. Zhao, Y.Z. Liu, H.M. Jiang, Q. Peng, J. Alloys Compd. 462 (2008) 103.
[22] S. Sagat, C.E. Coleman, M. Griffiths, B.J.S. Wilkins, in: Tenth Conference on Zirconium in the Nuclear Industry, ASTM STP 1245, ASTM, Philadelphia, 1994, p. 35.
[23] Y.S. Kim, Y.M. Cheong, J. Nucl. Mater. 373 (2008) 179.
[24] J. Tan, S.H. Ying, C. Li, C. Sun, Scripta Mater. 55 (2006) 513.
[25] Sun chao, Tan jun, Ying shihao, Li cong, Peng qian, Zhao suqiong, Acta Metall. Sin. 5 (2009) 541.
[26] S.Q. Shi, G.K. Shi, M.P. Plus, J. Nucl. Mater. 218 (1995) 189.
[27] L.A. Simpson, C.D. Cann, J. Nucl. Mater. 126 (1984) 70.
[28] B.A. Cheadle, C.E. Coleman, M. Ipohorski, in: Sixth Conference on Zirconium in the Nuclear Industry, ASTM STP 824, ASTM, Philadelphia, 1984, p. 210.
[29] C.E. Coleman, S. Sagat, K.F. Amouzouvi, in: 26th Annual Conference of 'Metallurgists Canadian Institute of Mining and Metallurgy', Atomic Energy of Canada Ltd., Report AECL-9524, 1987.
[30] C.E. Coleman, in: Fifth Conference on Zirconium in the Nuclear Industry, ASTM STP 754, ASTM, Philadelphia, 1982, p. 393.
[31] B. Cox, J. Nucl. Mater. 170 (1990) 1.
[32] A. Sawatzky, G.A. Ledoux, R.L. Tough, C.D. Cann, in: Proc. Miami Int. Symp. Metal–Hydrogen. Syst, Pergamon Press, Oxford, UK, 1982.
[33] S. Sagat, C.K. Chow, M.P. Puls, C.E. Coleman, J. Nucl. Mater. 279 (2000) 107.
[34] Sung Soo Kim, Young Suk Kim, J. Nucl. Mater. 279 (2000) 286.
[35] Young Suk Kim, Sang Chul Kwon, Sung Soo Kim, J. Nucl. Mater. 280 (2000) 304.
[36] S.S. Kim, S.C. Kwon, Y.S. Kim, J. Nucl. Mater. 273 (1999) 52.
[37] H. Huang, W.J. Mills, Metall. Trans. A 22A (1991) 2149.
[38] Young Suk Kim, Yuriy Perlovich, Margarita Isaenkova, Sung Soo Kim, Yong Moo Cheong, J. Nucl. Mater. 297 (2001) 292.